HHS Public Access

Author manuscript

Nat Struct Mol Biol. Author manuscript; available in PMC 2009 September 01.

Published in final edited form as:

Nat Struct Mol Biol. 2009 March ; 16(3): 312–317. doi:10.1038/nsmb.1560.

Structural basis for G9a-like protein lysine methyltransferase inhibition by BIX-01294

Yanqi Chang[1], **Xing Zhang**[1], **John R. Horton**[1], **Anup K. Upadhyay**[1], **Astrid Spannhoff**[2], **Jin Liu**[3], **James P. Snyder**[3], **Mark T. Bedford**[2], and **Xiaodong Cheng**[1]

[1]Departments of Biochemistry, Emory University School of Medicine, 1510 Clifton Road, Atlanta, GA 30322, USA

[2]M.D. Anderson Cancer Center, Department of Carcinogenesis, University of Texas, 1808 Park Road 1C, Smithville, Texas 78957, USA

[3]Department of Chemistry, Emory University, 324 Atwood, Atlanta, GA 30322, USA

Abstract

We present the crystal structure of the catalytic SET domain of G9a-like protein (GLP) in complex with BIX-01294. The inhibitor is bound in the substrate peptide groove at the location where the histone H3 residues (Lys4 to Arg8) N-terminal to the target lysine would occupy. The inhibitor is positioned in place by residues specific for G9a and GLP using planar stacking contacts, polar hydrogen bonds and van der Waals interactions.

Methylation of histone H3 at lysine 9 (H3K9) occurs in heterochromatin, which requires trimethylation of histone H3 at lysine 9 (H3K9me3) by Suv39h 1,2, and in euchromatin, which requires mono- and di-methylation of H3K9 (H3K9me1 and H3K9me2) mostly by G9a and GLP 3,4. H3K9me1 and H3K9me2 are the only silencing marks that are lost when tumor suppressor genes, e.g. in colorectal cancer cells 5 and in breast cancer cells 6, are reactivated following treatment with 5-aza-2'-deoxycytidine (5-aza), a DNA demethylation drug 7. Thus, the enzymes that produce H3K9me1 and H3K9me2 are appealing targets for inhibition. A small molecule, BIX-01294 (a diazepin-quinazolin-amine derivative), inhibits G9a enzymatic activity and reduces H3K9me2 levels at several G9a target genes 8. BIX-01294 was used as a replacement of Oct3/4 - one of the four original genetic factors used for reprogramming of mammalian somatic cells into induced pluripotent stem (iPS) cells 9 - in generating iPS cells from mouse fetal neural precursor cells 10, consistent with the observation that repressive H3K9 methylation by G9a is associated with Oct3/4 inactivation during differentiation 11.

Correspondence should be addressed to: Xiaodong Cheng, Phone: 404-727-8491, Fax: 404-727-3746, Email: xcheng@emory.edu.

Accession Codes. Protein Data Bank: The coordinates and structure factor for human GLP SET with bound BIX-01294 and AdoHcy have been deposited with accession number 3FPD.

Published online at http://www.nature.com/nsmb

Reprints and permissions information is available online at http://npg.nature.com/reprintsandpermissions/

RESULTS

BIX-01294 inhibits GLP as good as G9a

Here we show that the SET domain of human GLP (Supplementary Fig. 1) binds to BIX-01294 in a specific binding groove that prevents the peptide substrate from binding. We chose GLP to be the target of structural study for three reasons. First, the structure of GLP in complex with a H3 peptide substrate is available 12 (PDB 2RFI). Second, G9a and GLP share 80% sequence identity in their respective SET domains (Supplementary Fig. 2). Third, we found that BIX-01294 inhibits GLP as well or better than G9a (with IC_{50} values of 1.9 μM for G9a and 0.7 μM for GLP) when assayed under the linear reaction conditions (Fig. 1a–c). A previous report 8 that BIX-01294 inhibits GLP poorly (with IC_{50} of 38 μM) was conducted under conditions where the reaction was over-saturated, so that almost all substrate had been converted to trimethylated H3K9me3, a non-physiologically relevant product. In the same report 8, the G9a reaction was performed under conditions where mostly H3K9me1 and H3K9me2 were produced, and yielded similar IC_{50} to that observed here. In addition, K-ras mediated epigenetic silencing of the pro-apoptotic Fas gene, which can be reverted by 5-aza treatment 13 and RNAi mediated silencing of a number of epigenetic silencing effectors 14, is also reactivated by BIX-01294 treatment (Fig. 1d).

BIX-01294 occupies the binding site of histone peptide

BIX-01294 was soaked into a pre-formed crystal of binary complex of GLP SET domain with S-adenosyl-L-homocysteine (AdoHcy) (Fig. 2a) (Methods). We determined the ternary structure to a resolution of 2.42 Å (Table 1). G9a and GLP SET domains belong to the family of histone lysine methyltransferases (HKMTs) that contain Zn_3Cys_9 pre-SET and $ZnCys_3$ post-SET regions (Fig. 2a) 15–17}. The SET domain contains a series of curved β strands that surround a knot-like structure by threading the C-terminal post-SET (magenta) region through an opening of a short loop formed by a preceding stretch of the sequence (light blue) (Fig. 2a). The knot-like structure forms an active site immediately next to the methyl-donor-binding pocket (Fig. 2b) and the peptide-binding groove where BIX-01294 binds (comparing Fig. 2c and 2d). BIX-01294 lies in a location occupied by histone H3 Lys4-Arg8 (H3K4-H3R8) – the substrate sequence N-terminal to the target Lys9 – in the peptide complex 12 (PDB 2RFI) (Fig. 2e). The target lysine-binding channel is open with only a tip of the BIX-01294 molecule peeps through from the side (Fig. 2f). The AdoHcy sulfur atom, where the transferable methyl group would be attached on S-adenosyl-L-methionine (AdoMet), can be seen at the bottom of the channel.

BIX-01294 is bound to the acidic surface of the peptide-binding groove (Fig. 2b–d), sandwiched by helix αF-strands β10-β11 (bottom) and helix αZ (top) (Fig. 3a). The secondary structural elements of αF-β10-β11 are conserved among SET domains, while helix αZ (the last helix before the post-SET Zn binding) is unique to G9a and GLP (Supplementary Fig. 3). Other HKMTs have insertions in the corresponding regions (Supplementary Fig. 2), indicating selectivity could be achieved by targeting small molecules to these regions.

BIX-01294 resembles the bound conformation of H3K4 to H3R8

BIX-01294 consists of a central quinazoline ring linked to a seven-membered diazepane ring and a benzylated six-membered piperidine (Fig. 3b). The contacts between the enzyme and BIX-01294 are mostly concentrated on the quinazoline ring, its associated dimethoxy moieties, and the diazepane ring (Fig. 3b–3c). The branched benzene moiety has little direct contact with the enzyme. Thus the corresponding electron density is broken between the piperidine and benzyl moieties (Fig. 3d). Arg1214 and Ile1218 of helix αZ, Leu1143 of strand β10, Cys1155 of strand β11, and Ala1134 of helix αF provide van der Waals contacts with the quinazoline, the diazepane, and the amine linker between quinazoline and piperidine moieties (Fig. 3e). BIX-01294 is surrounded by four aspartates, Asp1131 and Asp1135 of helix αF, Asp1140 of the turn between helix αF and strand β10, and Asp1145 of strand β10 (Fig. 2b–2e) – all unique to G9a and GLP. Two of them, Asp1140 and Asp1145, having their negative charges balanced by interacting with Lys1219 and Arg1214, respectively (Fig. 2a, 2c), are within hydrogen bonding distance of the linker NH group between the quinazoline and piperidine rings and the ring nitrogen atom (N1) of the quinazoline ring, respectively. The close distance (3.0–3.2 Å) suggests that the carboxylate oxygen atoms of Asp1140 and Asp1145 are also able to form O···H-C type hydrogen bonds with the C5 and C8 of the quinazoline ring, repectively (Fig. 3b), a type of hydrogen bond that also occurs in the SET domain active sites 18. BIX-01294 could carry formal charge(s) if the diazepine N4 or the piperidine N1 is protonated. The close contact (2.7 Å) between Asp1131 and the diazepane ring N4 atom suggests the presence of a protonated cation and a hydrogen bond between Asp1131 and the N4-H (Fig. 3c), whereas the N1 of piperidine is distant away from Asp1135 and Asp1140 (~4.9 Å).

The ring based BIX-01294 superimposes well with the H3 peptide encompassing residues K4-R8 (PDB 2RFI 12; Fig. 2e). The reason for this mimicry is that the near perpendicular side chains of H3K4 and H3R8, stabilized by salt bridges with Asp1131, Asp1145, and Asp1135, allow the peptide to adopt a large square-like structure (Fig. 3f). An intra-molecular hydrogen bond between H3T6 and H3R8 further stabilizes the “square”. The side chain of H3R8 superimposes well with the entire left side of the quinazoline ring and the top half of the diazepane ring (Fig. 2e and colored green in Fig. 3b). The methyl group of the O6 methoxy mimics the side chain of H3A7 (colored red in Fig. 3b). Asp1140 forms analogous interactions with the NH group between quinazoline and piperidine moieties (color cyan) and the main chain amide nitrogen of H3A7. Finally, part of the piperidine ring mimics the conformation of main chain atoms between H3Q5 and H3T6 (Fig. 2e; colored cyan in Fig. 3b); and the 4-methyl-N4-C5 of diazepane mimics the side chain conformation of H3K4 (colored magenta in Fig. 3b). Taken together BIX-01294 resembles the bound conformation of peptide substrate histone H3K4 to H3R8. Note that neither the benzyl moiety of BIX-01294 nor the side chain of H3Q5 in the peptide have any direct interaction with and point away from the enzyme (Fig. 2e).

Conformational change of Arg1214 upon binding of BIX-01294

From the protein side, the biggest difference between the peptide-bound 12 and the BIX-bound structure is the side-chain conformation of Arg1214 (Fig. 3a). When the peptide substrate is bound, Arg1214 forms a salt bridge with Asp1217 of helix αZ. When the BIX is

bound, the guanidinium group of Arg1214 moves toward the compound and forms a salt bridge with Asp1145, replacing the salt bridge between Asp1145 and H3R8 when the peptide substrate was bound (Fig. 3f). The movement of Arg1214 also allows the hydrophobic portion of its side chain (and the rest of helix αZ) to stack with the quinazoline ring of BIX-01294, generating a large buried interface of 886 $Å^2$ between the enzyme and the compound, comparable to the interface between the enzyme and peptide substrate of H3K4-H3R8 (870 $Å^2$). The maximized shape complementarity between BIX-01294 and helix αZ, which is absent in other HKMTs, is primarily responsible for the selectivity of G9a and GLP over other methyltransferases examined 8. This selectivity is achieved despite the overall structural similarity of active sites (Supplementary Fig. 3).

BIX-01294 inhibits non-histone substrate

GLP and G9a also methylate non-histone substrates 19–21, including DNA methyltransferase 1 (DNMT1) (Fig. 1e, lanes 1 and 5). BIX-01294 is able to inhibit the methylation of DNMT1 by GLP and G9a (lanes 2–4 and 6–8), but not by Set7/9 (a protein methyltransferase 22,23) or DIM-5 (a H3K9me3 methyltransferase 15,16) that also methylate DNMT1 in vitro (lanes 9–14). These data indicate the inhibitor is enzyme specific rather than substrate specific. G9a, possibly GLP, mostly recognizes an Arg-Lys sequence 19 and the Arg side chain (the residue immediately preceding the target Lys) is the major site imitated by BIX-01294 (colored green in Fig. 3b), allowing the small molecule to inhibit fairly divergent substrates perhaps with varied potency.

DISCUSSION

The GLP SET-BIX structure is the first example of an inhibitor bound enzymatic SET domain structure of a HKMT. Comparison with the peptide-bound structure 12 illustrates similarity in their modes of binding, providing avenues for improving the potency and selectivity of the inhibitor. First, extending the branch of O7-methoxy-CH_3 into the target lysine-binding channel (Fig. 2f) should provide additional binding energy by increasing the surface area of binding. Second, placement of a reactive group near the seven-membered diazepane ring (e.g. a sulfhydryl group or a Michael acceptor) would allow for the formation of a covalent linkage with Cys1155; thereby enhancing inhibitor potency (Fig. 3e). Third, the apparent interaction between Asp1131 and the diazepane ring N4 - might be protonated at physiological pH (Methods) -suggest that inhibitor potency could be further improved by replacing the ring group with group(s) that better maximize the placement of complementary positively charged groups (Fig. 2b–c). Fourth, the benzyl moiety of the compound can be eliminated (if it does not affect the delivery of the compound across the cell membrane) or replaced with group(s) that maximizes the interaction with Asp1135. These modifications could increase the potency of this already proven important G9a/GLP inhibitor. In addition, the G9a/GLP-mediated DNMT1 methylation (Fig. 1e) adds one more dimension to the complex relationship between DNA methylation and G9a/GLP-mediated H3K9 methylation 24–26. BIX-01294 and its improved derivatives may ultimately allow for the generation of iPS cells in more chemically defined conditions, as well as treatment of cancer cells in conjunction with DNA methylation inhibitor(s).

METHODS

Protein purification

We obtained the expression constructs of human GLP (residues 951–1235) and G9a (residues 913–1193) from the Structural Genomics Consortium, University of Toronto. The N-terminal hexahistidine-tagged SET domain of human GLP residue 951–1235 (pXC681) or G9a residue 913–1193 (pXC682) was expressed in *Escherichia coli* BL21 (DE3)-Gold cells (Stratagene) with the RIL-Codon plus plasmid. Expression was induced with 0.4 mM isopropyl β-D-thiogalactoside for 16 h at 16°C in Luria-Bertani broth. The protein was isolated on a nickel-chelating column (GE Healthcare). After imidazole elution, the hexahistidine tag was cleaved by thrombin protease during overnight dialysis at 4 °C. Two extraneous N-terminal amino acids (GlySer) were fused to the N-terminal residues. The protein was further purified by ion exchange (HiTrap-Q) and gel filtration chromatography (Superdex-75 or -200, GE Healthcare).

Crystallography

The BIX-01294 dissolved in DMSO was soaked into preformed crystals of GLP-AdoHcy in the presence of DMSO. The purified GLP protein was incubated with AdoHcy at 1:2 molar ratio before concentrating to ~22 mg ml^{-1} in 20 mM Tris, pH 8.0, 400 mM NaCl, and 1% (v/v) glycerol. Clusters of needle (or rod)-shaped crystals were obtained using the hanging-drop vapor-diffusion method at 16 °C, with mother liquor containing 0.1 M HEPES pH 7.5, 18–20 % polyethylene glycol 4000 and 7–10 % isopropanol, in the absence or presence of DMSO (6–36%). BIX-01294 (ALEXIS) was dissolved in DMSO and kept in 20 mM stock. Preformed crystals were soaked into mother liquor supplemented with 6 mM BIX-01294 for 4 h (space group $P2_12_12_1$). X-ray diffraction data were collected, at the SER-CAT beamline APS-22BM, and processed with HKL2000 27, from crystals cyroprotected by the mother liquor supplemented with 25% ethylene glycol and flash frozen in liquid nitrogen.

We used the molecular replacement program PHASER 28 to obtain crystallographic phases using the coordinates of the binary structure of human GLP SET domain in complex with AdoHcy (PDB 2IGQ). The resulting electron density map for BIX-01294 and the structured portion of the two loops (residues 1146–1153 and 1220–1224) disordered in the binary structure was easily interpretable, using the model building program O 29. CNS 30 scripts were used for refinement. The statistics shown in Table 1 were calculated for the entire resolution range. The initial model of BIX-01294 and its topology parameters were generated by PRODRG 31. Because the current resolution of 2.42 Å is not sufficient to distinguish the chair vs. the boat conformations of the seven-membered diazepane ring and the six-membered piperidine ring, we constrained both rings in their chair conformations (which have lower energy than that of the boat conformations; see below). The R-free and R-work values were calculated for 5% (randomly selected) and 95%, respectively, of observed reflections. We assigned side chain of Arg1199 in two conformations, and manually assigned 119 water molecules with appropriate hydrogen bonds. The first 24-residues (951–974) were not assigned due to discontinued, residual densities.

There are two complexes (A and B) in the crystallographic asymmetric unit. While the protein components of the two complexes are highly similar, with root-mean-square deviation of less than 0.4 Å comparing 260 pairs of Cα atoms, the bound BIX molecule in complex B has lower thermal factors (40 vs. 53 $Å^2$) compare to that in complex A. The electron density is broken between the piperidine and benzyl moieties in complex B, whereas no density is observed for the benzyl moiety in complex A.

Mass spectrometry-based inhibition assay

Histone H3 peptide (residues 1–15) was used as substrates for G9a and GLP, under the conditions of 10 μM peptide, 100 μM AdoMet, 20 mM Tris pH 8.5, 5 mM dithiothreitol, and temperature at 30 °C. We first determined the linear range of the reaction for both enzymes in terms of enzyme concentration and reaction time (Fig. 1a). We chose the enzyme concentrations (0.03 μM of G9a and 0.12 μM of GLP) and reaction time of 7 min such that approximately 80% of the substrate peptide has been mono- or di-methylated, but not yet tri-methylated (a slow reaction for both enzymes 32), in the absence of inhibitors.

Inhibition assays were carried out by pre-incubating various concentrations of the inhibitor with the reaction mixture lacking the substrate on ice for 15 min followed by 5 min at 30°C. The reaction was started by addition of the substrate and stopped by addition of trifluoroacetic acid (TFA) to 0.1%.

For mass measurement, 1 μL of the reaction mixture with TFA was added directly to 1 μL saturated solution of a-cyano-4-hydroxycinnamic acid (CHCA) on a MTP 384 target plate (Bruker part no. 209520) and rapidly air-dried. Mass was measured by MALDI-TOF on a Bruker Ultraflex II TOF/TOF instrument (Biochemistry Department, Emory University School of Medicine) operated in reflective mode, externally calibrated with peptide calibration standard II (Bruker). Each measurement was the accumulation of three spectra collected at ten different positions with 600 shots per position (examples are shown in Supplementary Fig. 4). FlexAnalysis 3.0 software (Bruker Daltonik GmbH) was used to integrate area under each mass peak.

The sum of areas under each mass species gives rise to the total area of unmodified (me0), mono (me1), and di (me2)-methylated peptides, termed as A(n), n=0, 1, 2. The percentage of total area of intensity for each mass species, P(n) (n = 0, 1, 2), is calculated as $P(n) = 100 \times A(n) / [A(0)+A(1)+A(2)]$ (Fig. 1c). Methylation activity is defined as the number (N) of methyl groups added onto each peptide (Fig. 1a) and is calculated as $N(i) = [P(1) + 2 \times P(2)]/100$ under various concentrations of inhibitor (i). Note the di-methylation requires two rounds of methyl transfer. The percentage of inhibition is calculated as $I(\%) = 100 \times [1-N(i)/N(0)]$ (Fig. 1b). For each concentration of inhibitor, N(i) is the mean of two duplicated measurements. Untreated control N(0) is the mean value of six independent measurements. Curves were fit using Origin 7.0 software (OriginLab Corporation) in a sigmoidal fashion $[I(\%) = 100/(1+10^{(LogIC50-X)})]$ where X is the logarithm of concentration of BIX-01294.

Fas reactivation

K-ras NIH 3T3 transformed cells (ATCC, CRL-6361) were grown in Dulbecco's Modified Eagle Medium, 10% New Born Calf Serum. After 12 h the media was changed and the cells

were treated with BIX-01294 at 2.5 μM, 5-aza at 25 μM, or DMSO for 72 h. After the treatment the cells were lysed with 100 μl Radio Immunoprecipitation Assay buffer and sonicated for 5 s. After that, the samples were prepared for SDS-PAGE by boiling each sample with 25 μl loading buffer. The SDS-PAGE was performed on a 12.5% TRIS-HCl gel. The proteins were transferred to an Immobilon-P membrane (Millipore). Fas expression is monitored by immunoblot analysis. The anti-Fas antibody (Santa Cruz) was applied at a concentration of 1:100 in 5% dried milk / PBST 0.05% over night and detected using a HRP-labeled 2° antibody followed by ECL. Actin expression is shown as a loading control. Anti-actin antibody (Sigma-Aldrich) was used at 1:10,000.

Methylation of DNMT1

Reaction (20 μl) contained 1.1 μM purified human DNMT1 (expressed in *Pichia pastoris*), 2.8 μM [methyl-^{3}H]AdoMet, 1.8 μM enzyme (GLP, G9a, Set7/9 or DIM-5), and the indicated amount of BIX-01294 in 20 mM Tris (pH 8.5), and 5 mM dithiothreitol. The enzymes and the BIX compound were first incubated on ice for 15 min followed by 30°C for 5 min, then the reactions were started by addition of the substrate and lasted for 1.0–1.5 h at 30°C. Samples were analyzed by SDS-PAGE and fluorography and by precipitation with 10% trichloroaceitc acid (TCA) 15,16.

BIX-01294 pKa Values

The inhibitor structure was evaluated by the ACD pKa methodology 33 (www.acdlabs.com) produce pKa values of 8.94 and 8.79 for the piperidine N1 and the diazepane N4 nitrogen atoms, respectively. Close contact (2.7 Å) between the Asp1131 carboxylate and the diazepane N4 strongly suggests the presence of an ammonium cation at this center, affording an effective salt bridge (Fig. 3c). The benzylated N1 nitrogen is between both Asp1135 and Asp1140 with identical N…O distances of 4.9 Å.

BIX-01294 Conformations and Docking

To evaluate the relative energies of BIX-01294 conformations, the structure was built in 3D with the Spartan software (Wavefunction Inc., http://www.wavefun.com/) and optimized with MMFF/GBSA/H_2O 34 as the boat-boat, chair-boat and chair-chair conformations with respect to the piperidine and the diazepane rings. All structures with boat forms proved to be 6–11 kcal/mol high in energy relative to the chair-chair conformers, while the N4-Me axial forms raise the calculated energy by 3–5 kcal/mol. However, since there is precedence in the small molecule X-ray literature for axial NH^+-Me conformations 35 we decided to consider such forms in the ligand-protein docking.

There are four possible conformations involving the 1,4-diazepane ring, two arise by rotation around the C-N bond linking the quinazoline and diazepane rings (the asymmetric nature of the diazepane placing N4 in different locations in space), and two additional conformers result from populating the axial and equatorial N4-methyl forms. The lowest energy chair-chair conformer of BIX-01294 from the Spartan optimizations was transferred to Maestro 8.5.111 (Schrödinger, Inc., http://www.schrodinger.com/) and extra precision flexible Glide docking 36,37 of the N4 protonated forms (the axial-equatorial nature of the N4-methyl group) into the binding site of GLP was performed. Two N4-Me equatorial

conformers were observed with different spatial locations of the N-Me groups due to rotation about the C-N bond linking the quinazoline and diazepane rings. The NH^+-Me cation places the NH^+ functionality near Asp1131. The potential hydrogen bond between $N4^+$-H and Asp1131 (Fig. 3c) allows a rather straightforward selection of one of the chair-chair-equatorial conformers.

Supplementary Material

Refer to Web version on PubMed Central for supplementary material.

ACKNOWLEDGEMENTS

We thank Paul R. Thompson and Corey Causey for critical comments. The Biochemistry Department of Emory University School of Medicine supported the use of SER-CAT beamlines. This work was supported by grant GM068680 to X.C. from the National Institutes of Health and the Welch Foundation Grant G-1495 to MTB. X.C. is a Georgia Research Alliance Eminent Scholar.

References

1. Jenuwein T. The epigenetic magic of histone lysine methylation. Febs J. 2006; 273:3121–3135. [PubMed: 16857008]
2. Grewal SI, Jia S. Heterochromatin revisited. Nat Rev Genet. 2007; 8:35–46. [PubMed: 17173056]
3. Tachibana M, et al. G9a histone methyltransferase plays a dominant role in euchromatic histone H3 lysine 9 methylation and is essential for early embryogenesis. Genes Dev. 2002; 16:1779–1791. [PubMed: 12130538]
4. Tachibana M, et al. Histone methyltransferases G9a and GLP form heteromeric complexes and are both crucial for methylation of euchromatin at H3-K9. Genes Dev. 2005; 19:815–826. [PubMed: 15774718]
5. McGarvey KM, et al. Silenced tumor suppressor genes reactivated by DNA demethylation do not return to a fully euchromatic chromatin state. Cancer Res. 2006; 66:3541–3549. [PubMed: 16585178]
6. Wozniak RJ, Klimecki WT, Lau SS, Feinstein Y, Futscher BW. 5-Aza-2'-deoxycytidine-mediated reductions in G9A histone methyltransferase and histone H3 K9 di-methylation levels are linked to tumor suppressor gene reactivation. Oncogene. 2007; 26:77–90. [PubMed: 16799634]
7. Yoo CB, et al. Delivery of 5-aza-2'-deoxycytidine to cells using oligodeoxynucleotides. Cancer Res. 2007; 67:6400–6408. [PubMed: 17616700]
8. Kubicek S, et al. Reversal of H3K9me2 by a small-molecule inhibitor for the G9a histone methyltransferase. Mol Cell. 2007; 25:473–481. [PubMed: 17289593]
9. Takahashi K, Yamanaka S. Induction of pluripotent stem cells from mouse embryonic and adult fibroblast cultures by defined factors. Cell. 2006; 126:663–676. [PubMed: 16904174]
10. Shi Y, et al. A combined chemical and genetic approach for the generation of induced pluripotent stem cells. Cell Stem Cell. 2008; 2:525–528. [PubMed: 18522845]
11. Feldman N, et al. G9a-mediated irreversible epigenetic inactivation of Oct-3/4 during early embryogenesis. Nat Cell Biol. 2006; 8:188–194. [PubMed: 16415856]
12. Wu H, et al. Crystal structure of catalytic domain of human euchromatic histone methyltransferase 1 in complex with SAH and dimethylated H3K9 peptide. 2007 (PDB accession number 2RFI;
13. Peli J, et al. Oncogenic Ras inhibits Fas ligand-mediated apoptosis by downregulating the expression of Fas. Embo J. 1999; 18:1824–1831. [PubMed: 10202146]
14. Gazin C, Wajapeyee N, Gobeil S, Virbasius CM, Green MR. An elaborate pathway required for Ras-mediated epigenetic silencing. Nature. 2007; 449:1073–1077. [PubMed: 17960246]
15. Zhang X, et al. Structure of the Neurospora SET domain protein DIM-5, a histone H3 lysine methyltransferase. Cell. 2002; 111:117–127. [PubMed: 12372305]

16. Zhang X, et al. Structural basis for the product specificity of histone lysine methyltransferases. Mol Cell. 2003; 12:177–185. [PubMed: 12887903]
17. Cheng X, Collins RE, Zhang X. Structural and sequence motifs of protein (histone) methylation enzymes. Annual Review of Biophysics and Biomolecular Structure. 2005; 34:267–294.
18. Couture JF, Hauk G, Thompson MJ, Blackburn GM, Trievel RC. Catalytic roles for carbon-oxygen hydrogen bonding in SET domain lysine methyltransferases. J Biol Chem. 2006; 281:19280–19287. [PubMed: 16682405]
19. Rathert P, et al. Protein lysine methyltransferase G9a acts on non-histone targets. Nat Chem Biol. 2008; 4:344–346. [PubMed: 18438403]
20. Sampath SC, et al. Methylation of a histone mimic within the histone methyltransferase G9a regulates protein complex assembly. Mol Cell. 2007; 27:596–608. [PubMed: 17707231]
21. Pless O, et al. G9a-mediated lysine methylation alters the function of CCAAT/enhancer-binding protein-beta. J Biol Chem. 2008; 283:26357–26363. [PubMed: 18647749]
22. Chuikov S, et al. Regulation of p53 activity through lysine methylation. Nature. 2004; 432:353–360. [PubMed: 15525938]
23. Subramanian K, et al. Regulation of estrogen receptor alpha by the SET7 lysine methyltransferase. Mol Cell. 2008; 30:336–347. [PubMed: 18471979]
24. Dong KB, et al. DNA methylation in ES cells requires the lysine methyltransferase G9a but not its catalytic activity. Embo J. 2008; 27:2691–2701. [PubMed: 18818693]
25. Epsztejn-Litman S, et al. De novo DNA methylation promoted by G9a prevents reprogramming of embryonically silenced genes. Nat Struct Mol Biol. 2008; 15:1176–1183. [PubMed: 18953337]
26. Tachibana M, Matsumura Y, Fukuda M, Kimura H, Shinkai Y. G9a/GLP complexes independently mediate H3K9 and DNA methylation to silence transcription. Embo J. 2008; 27:2681–2690. [PubMed: 18818694]
27. Otwinowski Z, Borek D, Majewski W, Minor W. Multiparametric scaling of diffraction intensities. Acta Crystallogr A. 2003; 59:228–234. [PubMed: 12714773]
28. Storoni LC, McCoy AJ, Read RJ. Likelihood-enhanced fast rotation functions. Acta Crystallogr D Biol Crystallogr. 2004; 60:432–438. [PubMed: 14993666]
29. Jones TA, Zou JY, Cowan SW, Kjeldgaard M. Improved methods for building protein models in electron density maps and the location of errors in these models. Acta Crystallogr A. 1991; 47:110–119. [PubMed: 2025413]
30. Brunger AT. Crystallography & NMR system: A new software suite for macromolecular structure determination. Acta Crystallogr. D. 1998; 54:905–921. [PubMed: 9757107]
31. Schuttelkopf AW, van Aalten DM. PRODRG: a tool for high-throughput crystallography of protein-ligand complexes. Acta Crystallogr D Biol Crystallogr. 2004; 60:1355–1363. [PubMed: 15272157]
32. Collins RE, et al. In vitro and in vivo analyses of a Phe/Tyr switch controlling product specificity of histone lysine methyltransferases. J Biol Chem. 2005; 280:5563–5570. [PubMed: 15590646]
33. Meloun M, Syrovy T, Bordovska S, Vrana A. Reliability and uncertainty in the estimation of pKa by least squares nonlinear regression analysis of multiwavelength spectrophotometric pH titration data. Anal Bioanal Chem. 2007; 387:941–955. [PubMed: 17216158]
34. Halgren TA. MMFF VII. Characterization of MMFF94, MMFF94s, and other widely available force fields for conformational energies and for intermolecular-interaction energies and geometries. J Comput Chem. 1999; 20:730–748.
35. Seetharaman J, Rajan SS. Zeitschrift fuer krystallographie. 1995; 210:111–113.
36. Friesner RA, et al. Glide: a new approach for rapid, accurate docking and scoring. 1. Method and assessment of docking accuracy. J Med Chem. 2004; 47:1739–1749. [PubMed: 15027865]
37. Halgren TA, et al. Glide: a new approach for rapid, accurate docking and scoring. 2. Enrichment factors in database screening. J Med Chem. 2004; 47:1750–1759. [PubMed: 15027866]

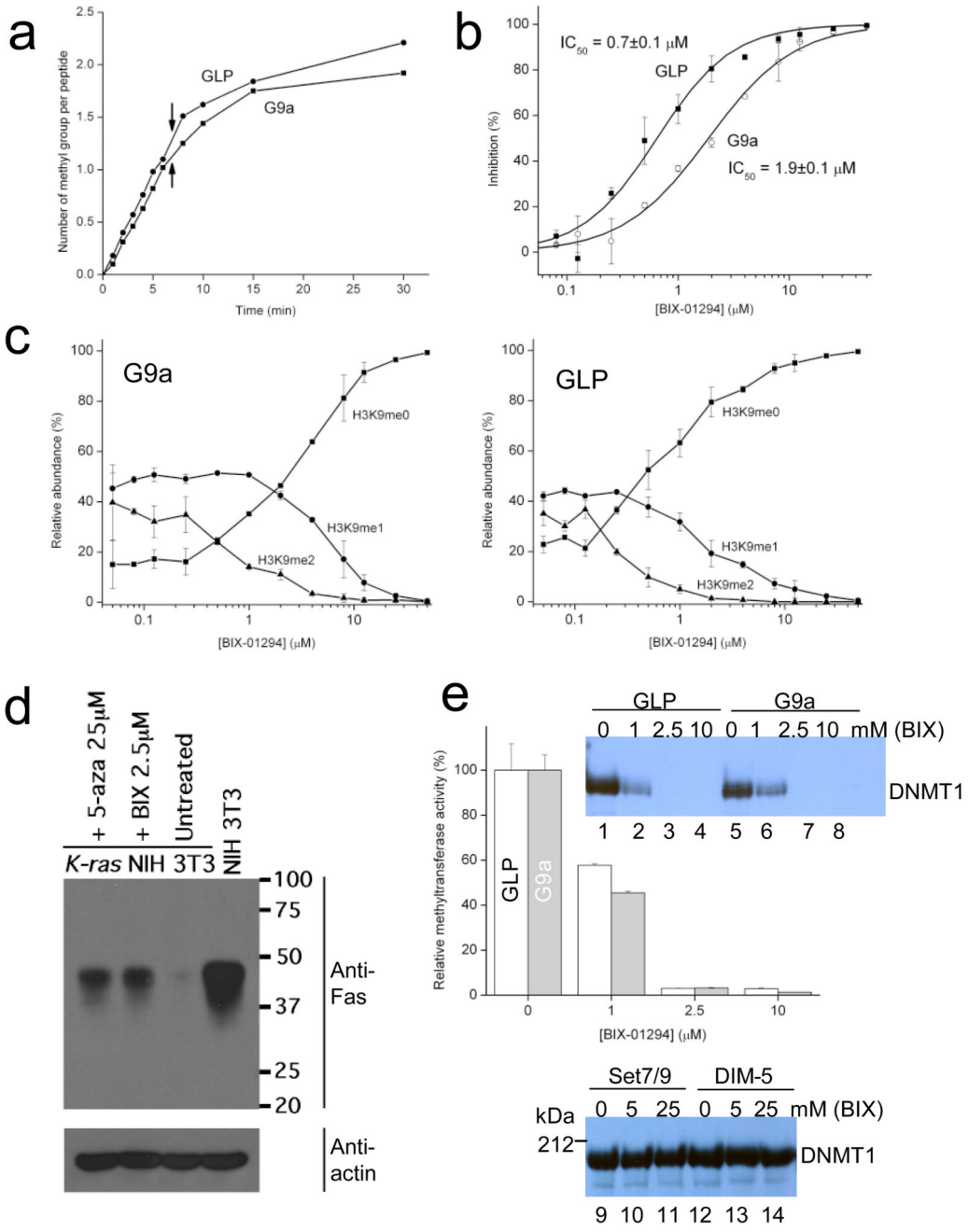

Figure 1. Effect of BIX-01294

(**a**) Progression of methylation as a function of reaction time. The arrows point to the conditions used for subsequent inhibition studies. (**b**) The inhibition on G9a and GLP by various concentrations of BIX-01294. (**c**) Variation in the relative abundance of each peptide species (me0, me1, and me2) as a function of BIX-concentration. (**d**) Ras-mediated epigenetic silencing of Fas is derepressed with both BIX-01294 and 5-aza treatments. (**e**) Methylation of DNMT1 by G9a and GLP and inhibition by BIX-01294; the autoradiography

image and relative activity by TCA counts. Error bars in panels b, c and e indicate s. d. for two duplicated measurements.

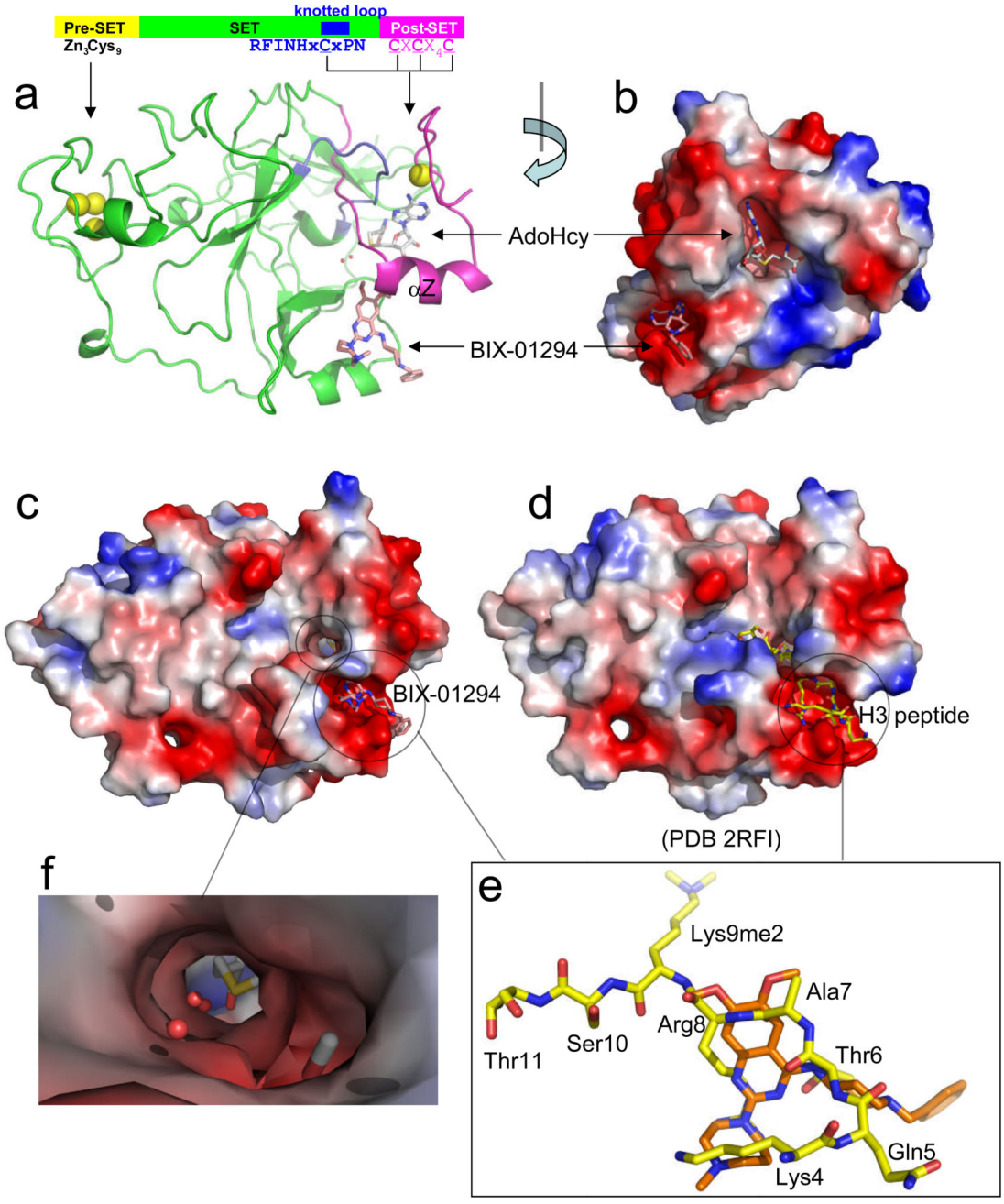

Figure 2. Structure of GLP SET-AdoHcy-BIX complex

(**a**) Structure of the GLP SET domain. (**b**) AdoHcy and BIX-01294 bind in two distinctive pockets. (**c** and **d**) BIX-01294 binds in the substrate peptide-binding groove (panel **c**), occupied by H3K4 to H3R8 (panel **d**; PDB 2RFI). (**e**) Superimposition of H3 peptide (yellow) and BIX-01294. (**f**) Water molecules (small red spheres) occupy the target lysine bind channel.

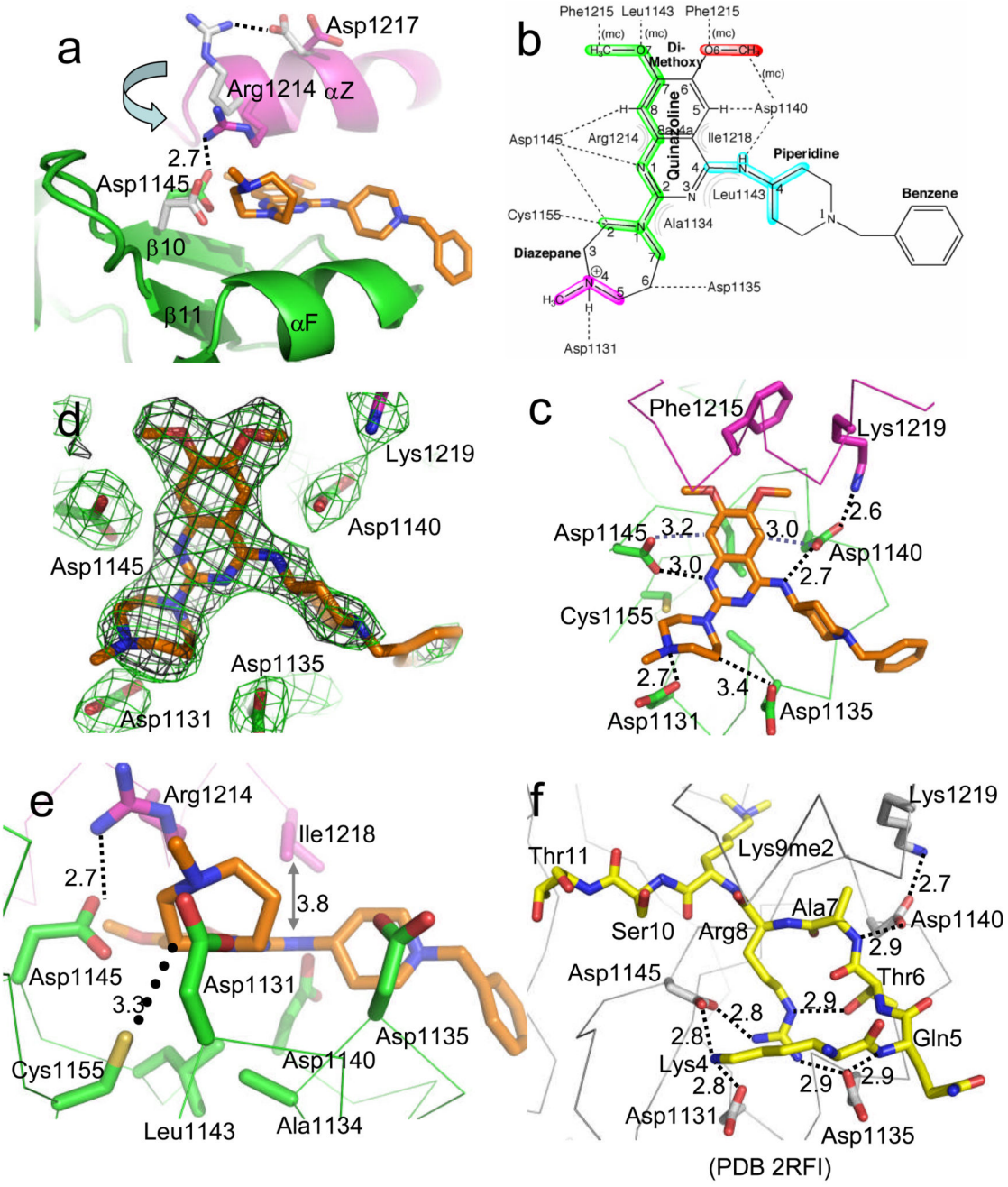

Figure 3. Details of GLP SET-BIX interactions

(**a**) Arg1214 undergoes large conformational change upon the binding of BIX-01294. (**b**) Summary of the SET-BIX interactions; mc, main-chain mediated contacts; dashed lines, hydrogen bonds; curved lines, hydrophobic contacts. (**c**) The hydrogen bonds with distances shown in angstroms. (**d**) Omit electron densities, Fo-Fc (red mesh) and 2Fo-Fc (green mesh), contoured at 4σ and 1.2σ above the mean, respectively, are shown for BIX-01294. (**e**)

Cys1155 interacts with diazepane ring. (**f**) Network of hydrogen bonds centered on histone H3K4 to H3R8 (PDB 2RFI).

Table 1

X-ray Data collection and refinement statistics (molecular replacement)

Data collection	**GLP SET-AdoHcy-BIX**	
Space group	$P2_12_12_1$	
Cell dimensions	(α=β=γ=90°)	
a (Å), b (Å), c (Å)	75.3, 95.2, 101.7	
Beamline	APS 22-BM (SER-CAT)	
Wavelength (Å)	1.00000	
Resolution (Å) *	30.26-2.42 (2.51-2.42)	
R_{merge} *	0.097 (0.430)	
I/σI *	10.3 (2.0)	
Completeness (%) *	91.7 (70.8)	
Redundancy *	4.4 (3.4)	
Observed reflections	116,317	
Unique reflections *	26,244 (1995)	
Refinement		
Resolution (Å)	2.42	
No. reflections	24,680	
R_{work} / R_{free}	0.221 / 0.262	
No. of atoms		
Protein	4154	
AdoHcy	52	
BIX	72	
Water	119	
Zn	8	
B-factors (Å^2)	39.4 (overall)	
Protein	molecule A	molecule B
	38.1	38.5
AdoHcy	58.2	51.2
BIX	52.8	40.2
Zn (pre/post-SET)	29.9/48.6	26.6/36.7
Water	37.7	
R.m.s. deviations		
Bond lengths (Å)	0.006	
Bond angles (°)	1.3	
Dihedral angles (°)	24.5	
Improper angles (°)	0.8	

* Highest resolution shell is shown in parenthesis.